CrystEngComm

PAPER

View Article Online
View Journal | View Issue

Cite this: *CrystEngComm*, 2015, **17**, 4161

Structural changes in M^{II} dithione/dithiolato complexes (M = Ni, Pd, Pt) on varying the dithione functionalization†

Davide Espa,[a] Luca Pilia,[ab] Luciano Marchiò,*[c] Salahuddin S. Attar,[a] Alberto Barsella,[d] Alain Fort,[d] Maria Laura Mercuri,[a] Angela Serpe[a] and Paola Deplano*[ae]

Received 6th March 2015,
Accepted 24th April 2015

DOI: 10.1039/c5ce00469a

www.rsc.org/crystengcomm

The Ni triad [M(R_2pipdt)(dmit)] based on donor/acceptor S,S′ ligands, where R_2pipdt = 1,4-diisopropyl-piperazine-2,3-dithione (acceptor) and dmit = 2-thioxo-1,3-dithiole-4,5-dithiolato (donor), was completed by preparing and characterizing the Pd(**2**) and Pt(**3**) compounds in addition to the already known Ni(**1**) complex. The rationale behind the work was to compare the properties and structures inside the triad with those of the corresponding Ni(**4**), Pd(**5**) and Pt(**6**) complexes where R = Bz. Minor changes in the properties as redox active nonlinear second-order (NLO) chromophores were observed in solution for the two triads. Instead, different structural features, reflected by changes in the diffuse reflectance spectra, were observed in their crystals on changing R from Bz to Pr^i in the piperazine ring and also, more surprisingly, inside the triads. **2** (isostructural with **1**) and **3** crystallized in monoclinic $P2_1/n$ and orthorhombic *Pbca* space groups, respectively. The crystal packings of **2** and **3** are also markedly different. In particular **1** and **2** form head-to-tail dimers whereas **3** forms supramolecular layers characterized by a partial stack between the molecular planes. Large differences in the crystal structures, induced by the diverse number and types of interactions exchanged by the peripheral fragments of the ligands, were found in the Bz-triad. Indeed, the molecules are stacked in a head-to-head and in a head-to-tail fashion in **4** and in **5**/**6**, respectively. Moreover, significantly different packings were observed. The Hirshfeld surface analysis was used to provide a detailed description of the main types of interactions involved in the crystal packing of the six complexes.

Introduction

Square-planar d^8 metal dithiolene complexes have been intensely investigated for their peculiar properties of interest in the fields of molecular materials exhibiting optical, conducting and magnetic properties.[1] The electronic properties of dithiolene complexes can be tuned by variation of substituents at the dithiolene core, and these terminal groups affect the highly delocalized frontier orbitals and related properties. In particular terminal groups attached to the dithiolene core with different electron withdrawing/donating capability induce a redistribution of the π-electrons in such a way that one of the ligands can be described as a dithione (acceptor), the other one as a dithiolato (donor). This behaviour is similar to what happens in the metal d^8 diimine–dithiolato complexes, where the acceptor is the diimine ligand.[2] These complexes behave as redox active second-order nonlinear chromophores showing high negative molecular first hyperpolarizability.[1d,3,4] An extensive experimental/theoretical investigation by our group by systematically varying the metal,[3,4] the dithione[4] and the dithiolato[3] ligands has allowed us to highlight the role that each component, *i.e.* donor, acceptor and metal ion, plays in tuning the properties of these complexes at the molecular level. It is found that mixed ligand complexes based on dithione (R_2pipdt = 1,4-dibenzyl-piperazine-2,3-dithione) and dithiolate ligands (dmit = 2-thioxo-1,3-dithiole-4,5-dithiolato) are the optimal candidates to achieve high second order NLO activity (see Scheme 1). Moreover, open-shell and closed-shell metal–dmit complexes

[a] *Dipartimento di Scienze Chimiche e Geologiche, Università di Cagliari, Unità di Ricerca dell'INSTM, S.S. 554-Bivio per Sestu, I09042 Monserrato-Cagliari, Italy. E-mail: deplano@unica.it*
[b] *Dipartimento di Ingegneria Meccanica Chimica e dei Materiali, Università di Cagliari, via Marengo 2, I09123, Cagliari, Italy*
[c] *Dipartimento di Chimica, Università di Parma, Parco Area delle Scienze 17A, I43100 Parma, Italy. E-mail: luciano.marchio@unipr.it*
[d] *Departement d'Optique ultra-rapide et Nanophotonique, IPCMS-CNRS, 23 Rue du Loess, BP 43, 67034 Strasbourg Cedex 2, France*
[e] *Dipartimento di Fisica, Università di Cagliari, S.S. 554-Bivio per Sestu, I09042 Monserrato-Cagliari, Italy*

† Electronic supplementary information (ESI) available: Fig. S1. Structural features of [Ni(Pr^i_2pipdt)(dmit)]; Fig. S2. Vis/NIR absorption spectra and solvatochromic behaviour of [Ni(Pr^i_2pipdt)(dmit)]; Fig. S3. Vis/NIR absorption spectra and solvatochromic behaviour of [Pd(Pr^i_2pipdt)(dmit)]; electrochemical measurements of [Pt(Bz_2pipdt)(dmit)]; Fig. S4. Hirshfeld surface for the three complexes [M(Pr^i_2pipdt)(dmit)] (M = Ni, Pd, Pt); Fig. S5. Hirshfeld surface for the three complexes [M(Pr^i_2pipdt)(dmit)] (M = Ni, Pd, Pt). See DOI: 10.1039/c5ce00469a

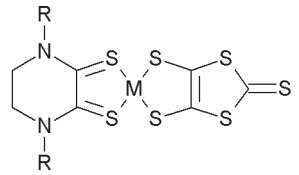

R_2pipdt dmit

R = Pr^i; M = Ni (**1**); Pd (**2**); Pt (**3**)
R = Bz; M = Ni (**4**); Pd (**5**); Pt (**6**)

Scheme 1

with similar ligands can form near infrared pigments, conducting or magnetic materials. In these systems the intermolecular interactions and stacking patterns govern the nature of these materials.[5]

Given the relevance of intermolecular interactions in determining the stacking patterns and related properties, we address this study mainly to reveal the structural features of [M(Pr^i_2pipdt)(dmit)] [Pr^i = isopropyl; M(II) = Ni (**1**), previously reported;[6] Pd (**2**); and Pt (**3**)] properties when compared to the corresponding complexes bearing Bz groups on the piperazine ring of the acceptor ligand, [M(Bz_2pipdt)(dmit)] (Bz: benzyl; M(II) = Ni (**4**),[6] Pd (**5**),[3e] and Pt (**6**)[3e]). The properties of these complexes are also compared in solution to support a predictable similar behaviour. Due to difficulties encountered in obtaining Pd and Pt compounds, as generally found when using the same synthetic procedure to prepare nickel-dithiolenes,[1,4] the influence of these substituents has been investigated previously for the nickel derivatives alone.[6] It was observed that when the Bz group[6] is present, the molecules are stacked in a one-dimensional columnar structure. Instead, in the Pr^i case,[3a] the Ni complex units are arranged head-to-tail forming dimers. Since palladium and platinum derivatives are currently available through an effective different synthetic procedure, it seemed interesting to us to deepen this investigation enlarging the comparison of crystal packing features on **1–6**. The Hirshfeld surface (HS) analysis[7] is an appropriate tool to investigate the packing features of a homologous series of compounds, and was employed to perform a thorough comparison of the packing in the six complexes, revealing the different types of interactions between the two [M(Bz_2pipdt)(dmit)]/[M(Pr^i_2pipdt)(dmit)] triads and inside each one of them.

Experimental section

Chemicals

Reagents and solvents of reagent grade and spectroscopic grade (DMF, CH_3CN and CS_2) have been used as received from Aldrich.

Preparations

[Ni(Pr^i_2pipdt)(dmit)] (1). **1** has been prepared following a procedure described in ref. 1*d*.

[Pd(Pr^i_2pipdt)(dmit)] (2). (n-Bu_4N)$_2$[Ni(dmit)$_2$] (114.83 mg) in 25 cm^3 of CH_3CN, green solution, was added dropwise to [Pd(Pr^i_2pipdt)](Cl)$_2$ (50.01 mg) in 25 cm^3 of CH_3CN, dark red suspension, under stirring. The solution, which turned to dark green immediately, was left under reflux for 24 h, and after that a precipitate was formed. The dark green precipitate was filtered, washed with diethyl ether, dried and recrystallized from DMF/diethyl ether (yield: 61.67 mg, 87%). CHNS: found (calcd for $C_{13}H_{18}N_2PdS_7$) C% 29.77 (29.28), H% 3.38 (3.40), N% 5.17 (5.25) S% 44.53 (42.10). FT-IR spectrum (cm^{-1}) 2928vw, 2206vs, 2187vw, 1635m, 1528vs, 1497vw, 1464w, 1454w, 1437m, 1357m, 1263w, 1184m, 1149w, 1109w, 1081w, 862vw, 738m, 698m, 605vw, 574w, 548w, 511w, 471w.

[Pt(Pr^i_2pipdt)(dmit)] (3). (n-Bu_4N)$_2$[Ni(dmit)$_2$] (107.28 mg) in 25cm^3 of CH_3CN, green solution, was added dropwise to [Pt(Pr^i_2pipdt)](Cl)$_2$ (50.00 mg) in 25 cm^3 of CH_3CN, dark red suspension, under stirring. The solution, which turned to dark green immediately, was left under reflux for 24 h, and after that a precipitate was formed. The dark green precipitate was filtered, washed with diethyl ether, dried and recrystallized from DMF/diethyl ether. Recrystallization from DMF/diethyl ether (yield: 66.64 mg, 94%). CHNS: found (calcd for $C_{13}H_{18}N_2PtS_7$) C% 25.39 (25.11); H% 2.46 (2.92); N% 4.50 (4.51); S% 39.14 (36.09). FT-IR spectrum (cm^{-1}) 2967vw, 2927vw, 1645vs, 1508vs, 1428vs, 1378m, 1356m, 1276w, 1251w, 1240w, 1190w, 1108s, 1049s, 1024s, 904m, 720w, 587w, 511w, 475w.

Microanalyses were performed by means of a Carlo Erba CHNS Elemental Analyzer model EA1108.

Spectroscopic and electrochemical measurements. I.R. spectra (4000–350 cm^{-1}) were recorded on a Bruker IFS55 FT-IR Spectrometer as KBr pellets. Electronic spectra were recorded with a Cary 5 spectrophotometer. Cyclic voltammograms were recorded on a EG&G (Princeton Applied Research) potentiostat-galvanostat model 273, by using a conventional three-electrode cell consisting of a platinum wire working electrode, a platinum wire as counter-electrode and Ag/AgCl in saturated KCl solution as reference electrode. The experiments were performed at room temperature (25 °C), in a dry and argon-degassed DMF containing 0.1 mol dm^{-3} Bu_4NBF_4 as supporting electrolyte, in the 20–100 mV s^{-1} scan rate range.

NLO measurements. EFISH experiments have been performed using a freshly prepared 10^{-3} M solution in DMF and working with a 1907 nm incident wavelength, obtained by Raman shifting the 1064 nm emission of a Q-switched Nd:YAG laser in a high pressure hydrogen cell (50 bar). A liquid cell with thick windows in the wedge configuration has been used to obtain the Maker fringe pattern (harmonic intensity variation as a thickness of liquid traversed). In the EFISH experiments the incident beam (6 ns pulses with 10 Hz repetition rate) has been synchronized with a DC field applied to the solution (5 μs duration) in order to break its centrosymmetry. From the concentration dependence of the harmonic signal with respect to that of the pure solvent, the NLO responses have been determined (assumed to be real because the imaginary part has been neglected) from the experimental value γ_{EFISH} through eqn (1):

$$\gamma_{\mathrm{EFISH}} = \frac{\mu\beta_{\lambda}(-2\omega;\omega,\omega)}{5kT} + \lambda(-2\omega;\omega,\omega,0) \quad (1)$$

where λ_{EFISH} is the sum of a cubic electronic contribution $\gamma(-2\omega;\ \omega,\ \omega,\ 0)$, which is neglected, and of a quadratic orientational contribution $\mu\beta_{\lambda}(-2\omega;\ \omega,\ \omega)/5kT$, being μ the ground state dipole moment, and β_{λ} the projection along the dipole moment direction of the vectorial component β_{vec} of the tensorial quadratic hyperpolarizability working with the incident wavelength λ.

X-ray data collection and structure determination

A summary of data collection and structure refinement for [Pd(Pr^i_2pipdt)(dmit)] (2) and [Pt(Pr^i_2pipdt)(dmit)] (3) is reported in Table 1. Single crystal data were collected with a Bruker Smart 1000 area detector diffractometer, Mo Kα: λ = 0.71073 Å. The unit cell parameters were obtained using 60 ω-frames of 0.5° width and scanned from three different zones of reciprocal lattice.

The intensity data were integrated from several series of exposure frames (0.3° width) covering the sphere of reciprocal space.[8] An absorption correction was applied using the program SADABS[9] with min. and max. transmission factors of 0.856–1.000 (2) and 0.487–1.000 (3). The structure was solved by direct methods (SIR97 [10]) and refined on F^2 with full-matrix least squares (SHELXL-97 [11]), using the Wingx software package.[12,13] Nonhydrogen atoms were refined anisotropically and the hydrogen atoms were placed at their calculated positions. The graphical material was prepared with the Mercury 3.0 [14] program. CCDC 1040215–1040216 contain the supplementary crystallographic data for this paper.

Hirshfeld surface analysis. The Hirshfeld surface (HS) properties[7,15] were computed with the CrystalExplorer 3.0 program[16] in order to elucidate the differences and similarities between the packing modes for the six complexes. The HS defines the volume of space in a crystal where the sum of the electron density of the spherical atom for the molecule (pro-molecule) exceeds that for the crystal (pro-crystal). Various properties of the HS can be computed and visualized, in particular d_e and d_i, which represent the distance from a point on the surface to the nearest nucleus outside or inside, respectively, the surface. The d_{norm} is the normalized contact distance and is defined by taking into account d_e and d_i and the van der Waals radii of the atoms:

$$d_{\mathrm{norm}} = \frac{d_i - r_i^{\mathrm{vdW}}}{r_i^{\mathrm{vdW}}} + \frac{d_e - r_e^{\mathrm{vdW}}}{r_e^{\mathrm{vdW}}}$$

d_{norm} can be mapped on the HS providing clear evidence of the interactions exchanged by the adjacent molecular fragment (visualized as red spots on the HS). Moreover, the correlation between d_e and d_i provides the fingerprint plots, which are 2D diagrams that provide a thorough depiction of the overall interactions exchanged by the molecules within the crystal.[17]

Table 1 Summary of X-ray crystallographic data for [Pd(Pr^i_2pipdt)(dmit)] (2) and [Pt(Pr^i_2pipdt)(dmit)] (3)

	[Pd(Pr^i_2pipdt)(dmit)]	[Pt(Pr^i_2pipdt)(dmit)]
Empirical formula	$C_{13}H_{18}N_2PdS_7$	$C_{13}H_{18}N_2PtS_7$
Formula weight	533.11	621.80
Crystal size (mm)	0.20 × 0.15 × 0.10	0.32 × 0.12 × 0.10
Crystal system	Monoclinic	Orthorhombic
Space group	$P2_1/n$	*Pbca*
a, *b*, *c* (Å)	9.687(2), 17.320(5), 12.544(3)	14.578(1), 16.218(1), 16.257(1)
α, β, γ (deg.)	90, 108.034(7), 90	90, 90, 90
V (Å^3)	2001.2(9)	3843.6(4)
Z	4	8
T (K)	293 (2)	200(2)
ρ(calc) (Mg/m^3)	1.769	2.149
μ (mm^{-1})	1.656	8.060
θ range (deg.)	2.07 to 28.03	2.26 to 27.03
No. of rflcn/obsv ($I > 2\sigma(I)$)	24 254/4810	41 982/4218
GooF	1.005	1.009
R_1 [a]	0.0289	0.0294
wR_2 [b]	0.0673	0.0641

[a] $R_1 = \sum||F_o| - |F_c||/\sum|F_o|$. [b] $wR_2 = [\sum[w(F_o^2 - F_c^2)^2]/\sum[w(F_o^2)^2]]^{1/2}$, $w = 1/[\sigma^2(F_o^2) + (aP)^2 + bP]$, where $P = [\max(F_o^2,0) + 2F_c^2]/3$.

Results and discussion

Synthesis

[M(II)(Pr^i_2pipdt)(dmit)], [M(II) = Pd (2); Pt (3)], has been obtained by reacting [M(II)(Pr^i_2pipdt)Cl_2] with $(Bu_4N)_2$[Ni(II)$(dmit)_2$] as shown in Scheme 2.

Salts of nickel dianionic complexes provide the required dianion, which when uncoordinated is less stable, to form the desired mixed-ligand complexes in high yields (80–90%) with respect to the [M(Pr^i_2pipdt)Cl_2] reagent, accompanied by Bu_4NCl and degradation products containing the nickel cations. On slow evaporation of the solvents, well-formed dark crystals precipitated.

X-ray structures

The molecular structures of [Pd(Pr^i_2pipdt)(dmit)] (2) and [Pt(Pr^i_2pipdt)(dmit)] (3) are reported in Fig. 1. Despite the very similar molecular structures the two compounds crystallize in different space groups, monoclinic $P2_1/n$ for 2 and orthorhombic *Pbca* for 3. The metal geometry is square planar according to the

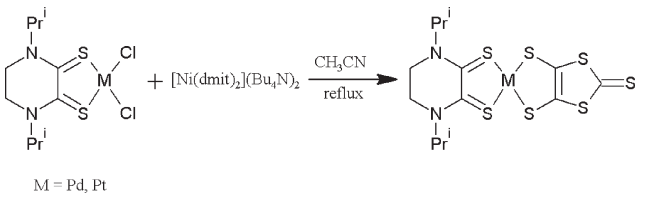

Scheme 2

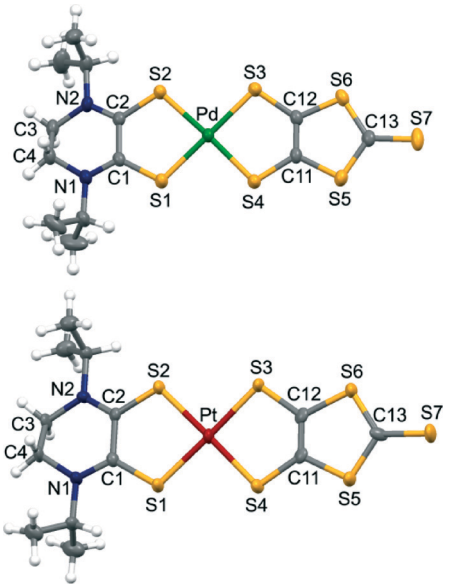

Fig. 1 Molecular structures of [Pd(Pr$^i_2$pipdt)(dmit)] (**2**) (above) and of [Pt(Pr$^i_2$pipdt)(dmit)] (**3**) (below) with thermal ellipsoids drawn at the 30% probability level.

Table 2 Selected bond distances (Å) and angles (°) for **2** and **3**

2		**3**	
Pd–S(1)	2.2714(9)	Pt–S(1)	2.275(1)
Pd–S(2)	2.2837(8)	Pt–S(2)	2.275(1)
Pd–S(3)	2.296(1)	Pt–S(3)	2.279(1)
Pd–S(4)	2.2842(8)	Pt–S(4)	2.284(1)
C(1)–S(1)	1.685(3)	C(1)–S(1)	1.702(5)
C(2)–S(2)	1.696(3)	C(2)–S(2)	1.701(5)
C(11)–S(4)	1.729(3)	C(11)–S(4)	1.713(5)
(12)–S(3)	1.743(3)	C(12)–S(3)	1.730(5)
C(1)–C(2)	1.489(4)	C(1)–C(2)	1.490(6)
C(11)–C(12)	1.343(4)	C(11)–C(12)	1.287(7)
S(1)–Pd–S(2)	87.96(3)	S(1)–Pt–S(2)	87.74(5)
S(1)–Pd–S(4)	89.39(3)	S(1)–Pt–S(4)	90.72(5)
S(2)–Pd–S(3)	91.48(3)	S(2)–Pt–S(3)	90.41(4)
(3)–Pd–S(4)	91.14(3)	S(3)–Pt–S(4)	91.13(5)
C(1)–S(1)–Pd	106.4(1)	C(1)–S(1)–Pt	106.5(2)
(2)–S(2)–Pd	105.3(1)	C(2)–S(2)–Pt	106.2(2)
C(12)–S(3)–Pd	100.21(9)	C(12)–S(3)–Pt	99.2(2)
(11)–S(4)–Pd	100.83(9)	C(11)–S(4)–Pt	99.8(2)

presence of four sulphur atoms from two S,S bidentate ligands. The geometry of **2** and **3** is more regular than that reported for strictly related compounds, namely [Pd(Me$_2$pipdt)(dmit)],[18] [Pd(Bz$_2$pipdt)(dmit)] and [Pt(Bz$_2$pipdt)(dmit)],[3e] in which the dihedral angle between the *dithione-M* and *dithiolate-M* coordination plane varies between 4° and 8°, whereas in **2** and **3** it is 2° and 1°, respectively.

The metal–sulphur bond distances are in the relatively narrow ranges of 2.2714(9)–2.296(1) Å (**2**) and 2.275(1)–2.284(1) Å (**3**), so that it is not possible to correlate the M–S separation with the electronic properties of the Pr^i-pipdt (dithione) and dmit (dithiolate) ligands in each complex. On the other hand, the C–S bond distances more appropriately reflect the different nature of the ligands, since in the dithione they are significantly shorter than in the dithiolate, Table 2. Moreover, the C–C bond linked to the coordinated sulphur atoms exhibits a double bond character for the dmit and a single bond character for the Pr^i-pipdt ligands. Since the properties of a material are strongly influenced by the structural arrangements of the molecules within the crystal lattice, in the present case it is interesting to compare the crystal packing features of (**2**) and (**3**) with those exhibited by [Pd(Bz$_2$pipdt)(dmit)] (**5**) and [Pt(Bz$_2$pipdt)(dmit)] (**6**).[3e]

Complexes **1** and **2** are isostructural therefore their overall features can be described together (Fig. S1 and S2†). On the other hand, the crystal packing of **2** and **3** is markedly different, as can be appreciated by comparing Fig. 2 and 3. In **2**, two complex molecules are stacked in a head-to-tail fashion and the shortest contact is exhibited by the S(7) and C(1)′ atoms of two molecules (3.40 Å, ′ = 1 − x; 1 − y; 1 − z). The Pd atom is partly overlying with the peripheral C═S moiety of dmit and the methyl and one molecule (C–H$_{methyl}$···C(13) = 2.80 Å, C–H$_{methylene}$···S(7), = 2.92 Å). According to the presence of these interactions, the dimeric units are arranged nearly perpendicular to each other in the crystal packing, see Fig. 2. The crystal packing of **3** is rather different, in fact the complex molecules are partially stacked above each other by virtue of a series of interactions exchanged by the dmit ligand and the aliphatic groups of the Pr$^i_2$pipdt ligands of adjacent molecules (see Fig. 3).

These contacts lead to the formation of supramolecular layers that run parallel to the *bc* crystallographic plane and the layers exchange hydrophobic interactions by means of the Pr^i residues of the Pr$^i_2$pipdt ligand.

The substitution of the i-propyl residue of Pr$^i_2$pipdt with the benzyl group in Bz$_2$pipdt modifies the number and types of interactions that can be exchanged by the peripheral fragments of the ligands. In particular, the presence of the aromatic rings introduces the possibilities of π···π stacking as well as CH···π interactions. This in fact is evident in the crystal structure of **5** and **6**, where the molecules are arranged in a head-to-tail columnar stacking and the supramolecular interactions between the columns are derived from the π···π stacking of the benzyl residues, Fig. 4 and 5.

The packing within each column is slightly different for **5** and **6**. In fact, in **5** the Pd atoms of one molecule are located above the chelation ring of the Bz$_2$pipdt with the minimum distances exhibited by the metal and the sulphur atoms (Pd···S(2)′ = 3.71 Å, ′ = −x; −y; 1 − z; Pd···S(1)″ = 3.71 Å, ″ = 1 − x; −y; 1 − z). In **6**, the metal lies between two hexa-atomic rings of the Bz$_2$pipdt ligands with the minimum distances exhibited by the metal and the nitrogen atoms (Pt···N(2)′ = 3.73 Å, ′ = −x; 1 − y; −z; Pt···N(1)″ = 3.73 Å, ″ = 1 − x; 1 − y; −z). Within the columnar stack, in **6** the molecules exhibit a more pronounced shift of the coordination planes with respect to **5** that together with the different orientation of the benzyl groups influences the packing modes of the two compounds: 1) in **6** the columns interact more strongly through the peripheral sulphur atoms and the CH$_2$ groups of

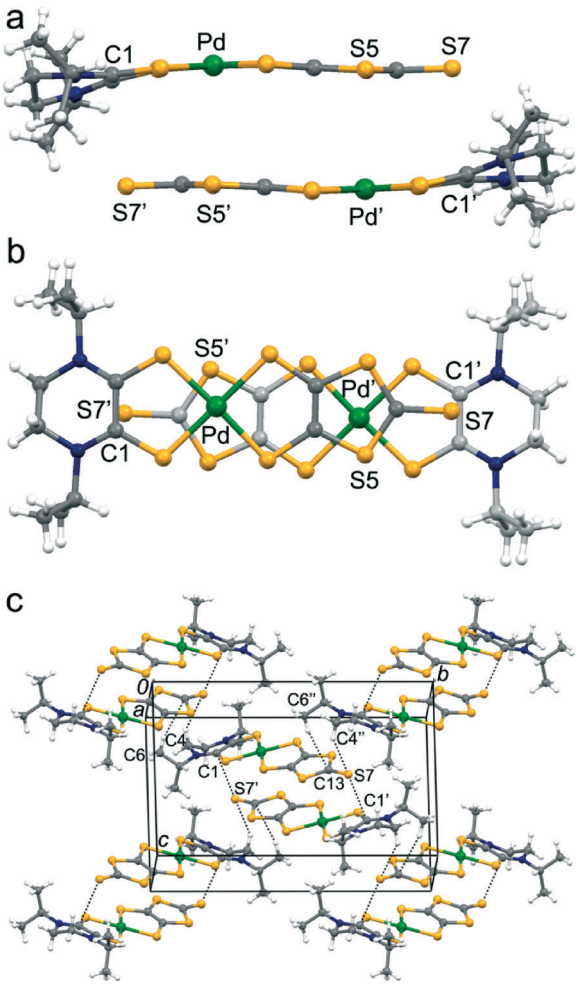

Fig. 2 Depiction of the dimer formed by two stacked [Pd(Pr$^i_2$pipdt)(dmit)] molecules, side view (a), top view (b). Crystal packing of [Pd(Pr$^i_2$pipdt)(dmit)] projected along the *a* axis. Dashed bonds indicate short contacts (c). Symmetry codes ′ = 1 − *x*; 1 − *y*; 1 − *z*, ″ = 1/2 − *x*; 1/2 + *y*; 1/2 − *z*.

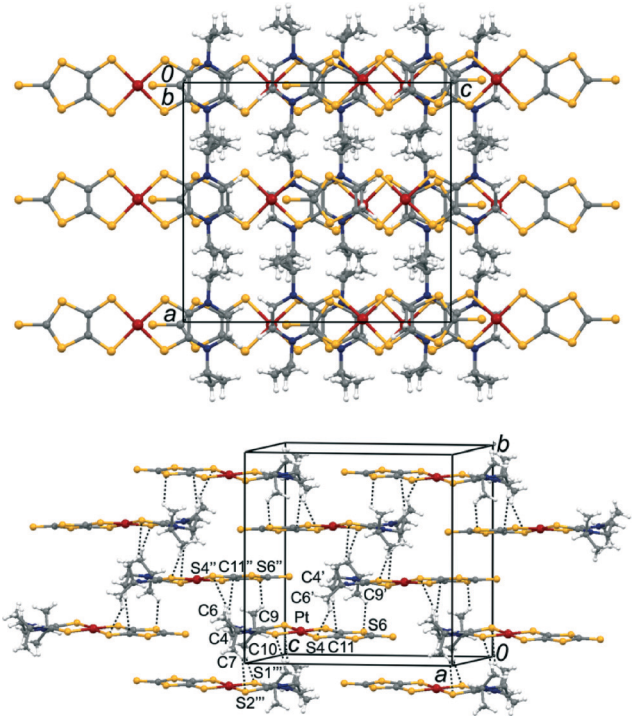

Fig. 3 Crystal packing of [Pt(Pr$^i_2$pipdt)(dmit)] projected along the *a* axis (above) and along the *b* axis (below). Dashed bonds indicate short contacts. Symmetry codes ′ = *x*; 1/2 − *y*; *z* − 1/2, ″ = *x*; 1/2 − *y*; 1/2 + *z*, ‴ = 1 − *x*; −*y*; 2 − *z*.

the Bz$_2$pipdt ligands, and 2) within the stack, the benzyl residues of one molecule are interacting with the sulphur atoms involved in the metal coordination of an overlaid complex molecule. A significantly different packing is exhibited by **4** (Fig. 6), where the molecules are stacked in a head-to-head fashion with the Ni atom that is located between the CH_2 of the hexa-atomic ring and the peripheral C═S residue of Bz$_2$pipdt and dmit ligands (Ni···H(2)′ = 2.68 Å, ′ = *x*; *y*; *z* − 1; Ni···C(2)″ = 3.67 Å, ″ = *x*; *y*; *z* + 1). Moreover, the benzyl residues in **4** are oriented on the same side of the molecular plane at variance with the structure of **5** and **6** where the same groups are oriented on opposite sides. As a consequence, the interactions exchanged by the benzyl moieties in **4** and **5**/**6** are markedly different. The extensive net of π···π stacking in **5**/**6** is no longer present in **4**, in which adjacent columns interact through the aromatic rings and the sulphur atoms involved in the metal coordination (C(10)‴···S(1) = 2.987 Å, ‴ = 1 − *x*; 1 − *y*; 1 − *z*). Furthermore, in **4** the molecules belonging to different stacks are oriented in a V fashion with the angle between the mean molecular planes approximately 73°.

A thorough comparison between the packing of the six complexes can be obtained by inspecting the fingerprint plots derived from the Hirshfeld surface analysis, Fig. 7. For all complexes the main types of interactions are those involving the hydrogen and the sulphur atoms. Despite the fact that **1** and **2** are isostructural there are some differences between their fingerprint plots and this may be a consequence of the shorter coordination bond length in **1** with respect to **2**, causing some modification of the overall crystal packing between the molecules. It is also interesting to note that the interactions involving the sulphur atoms are more important for **1**–**3** than for **4**–**6**. In addition in **4**–**6** a significant fraction of the interactions exchanged by the molecules comprises the carbon atoms, in agreement with the presence of a significant number of π···π and CH···π interactions exchanged by the benzyl residues. For the sake of completeness it should be mentioned that in similar molecular systems, the use of the Fukui functions was proposed as a valuable tool for the identification of the potential sites of interactions between adjacent molecules in the solid state.[2d]

Visible absorption spectroscopy and EFISH data

Complexes **1**–**3** are characterized in the visible region by a highly negative solvatochromic band broad peak. This band

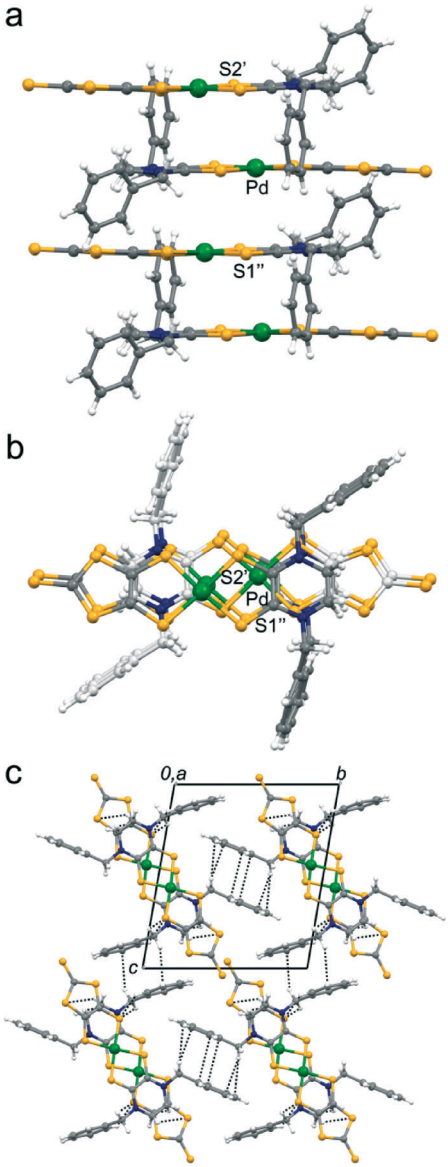

Fig. 4 Portion of the molecular stack of [Pd(Bz$_2$pipdt)(dmit)], side view (a), top view (b). Symmetry codes ′ = −*x*; −*y*; 1 − *z*. ″ = 1 − *x*; −*y*; 1 − *z*. Crystal packing of [Pd(Bz$_2$pipdt)(dmit)] projected along the *a* axis (c). Dashed bonds indicate short contacts. Color code: Pd, green, S, yellow, C, gray, H, white, N, blue.[3e]

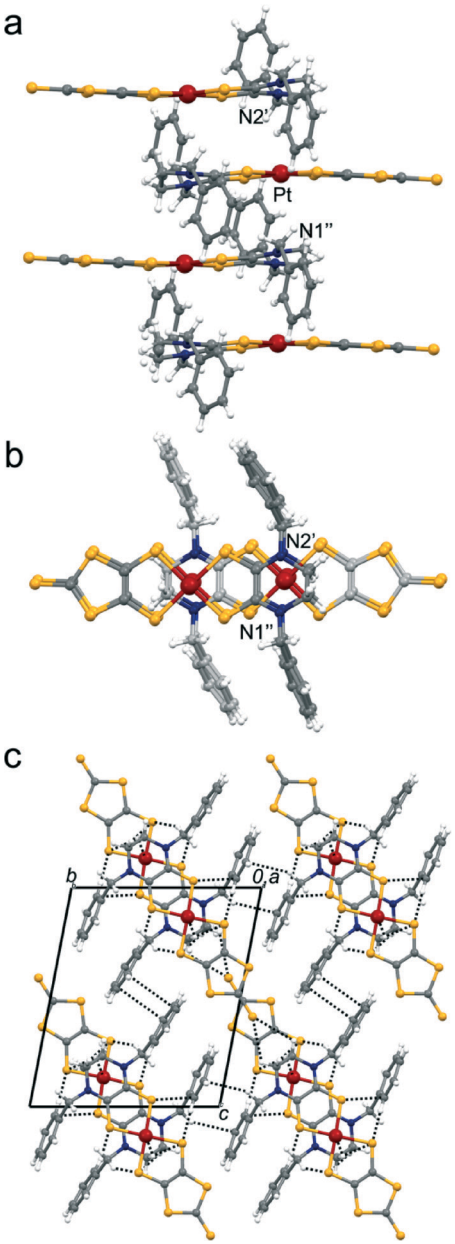

Fig. 5 Portion of the molecular stack of [Pt(Bz$_2$pipdt)(dmit)],[3e] side view (a), top view (b). Symmetry codes ′ = −*x*; 1 − *y*; −*z*. ″ = 1 − *x*; 1 − *y*; −*z*. Crystal packing of [Pt(Bz$_2$pipdt)(dmit)] projected along the *a* axis (c). Dashed bonds indicate short contacts. Color code: Pt, scarlet, S, yellow, C, gray, H, white, N, blue.[3e]

is accompanied by a second one, which appears either as a shoulder in the high-energy edge or just widens the main band (Fig. S4†). The wavelengths of these two components have been determined by deconvolution of the overlapping bands and are reported in Table 3. Results from time-dependent density functional theory (TD-DFT) calculations[3b,4] suggest that the first band can be assigned to a mixed metal-ligand-to-ligand charge-transfer transition (MMLL'CT) and can be up to a point described as a HOMO → LUMO one, where the HOMO is formed by a mixture of metal and dithiolate orbitals while dithione orbitals give a predominant contribution to the LUMO. On the other hand, the populated state has a slight multiconfigurational character, since the contribution of the latter is predominant but not unique. The shoulder at higher energy is the relatable HOMO-1 → LUMO transition, where the HOMO-1 is formed by a mixture of metal, dithiolate and dithione orbitals, but the very low value of the oscillator strength of this transition can make this peak not observable.[3c,4]

EFISH experiments, as described in the Experimental section, allowed determination of the scalar product $\mu\beta_\lambda$ (μ = ground state dipole moment; β_λ = projection of the vectorial component of the quadratic hyperpolarizability tensor along the dipole moment axis). The $\mu\beta_\lambda$ values determined at 1907

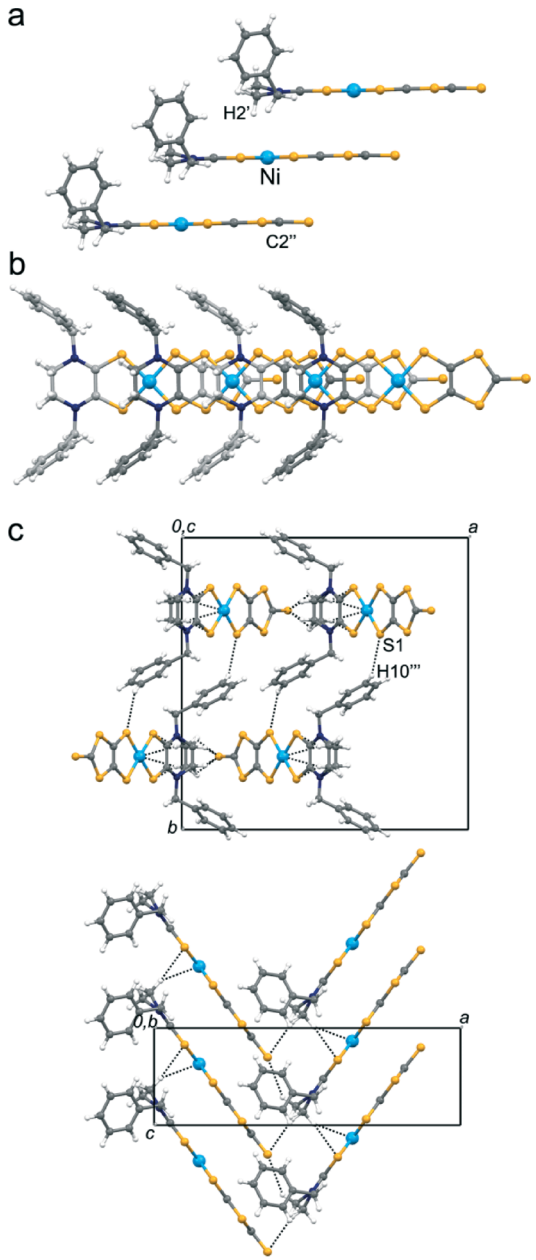

Fig. 6 Portion of the molecular stack of [Ni(Bz$_2$pipdt)(dmit)],[6] side view (a), top view (b). Crystal packing of [Ni(Bz$_2$pipdt)(dmit)] projected along the *c* axis and along the *b* axis (c). Dashed bonds indicate short contacts. Color code: Ni, light blue, S, yellow, C, gray, H, white, N, blue.

nm incident wavelength are listed in Table 3, and can be extrapolated to zero frequency by applying the equation: $\beta_0 = \beta\lambda[1 - (2\lambda_{max}/\lambda)^2][1 - (\lambda_{max}/\lambda)^2]$ giving for $\mu\beta_0$ (10^{-48} esu) −1247 (−1089) (**1**), −1332 (−938) (**2**), and −1896 (−1735) (**3**). In italics the values obtained with λ_{max} result in deconvolution of the broad band. Given the high approximation in their determination, the obtained values can be considered roughly comparable with those determined for **4–6** [$\mu\beta_0$(10^{-48} esu) −926 (**4**); −1146 (**5**); −1804 (**6**)] suggesting that the substitution of Bz groups with Pr^i ones in R$_2$pipdt does not affect significantly the second-order NLO response in the [M(R$_2$pipdt)(dmit)] complexes, and confirm that the largest value is found for the platinum complex. A β_0 value of −130 × 10^{-30} esu has been determined for **1** by a solvatochromic method.[1d]

Notably, the $\mu\beta_0$ values of these mixed-ligand dithiolene complexes are among the highest values so far reported for metal complexes and are also high compared to those of organic second-order NLO chromophores.[19]

Previous theoretical studies have shown that the remarkable first molecular hyperpolarizability of metal R$_2$pipdt/dmit derivatives can be attributed, in addition to a high difference in dipole moments between excited and ground state and the low energy of the charge transfer transition, both to the lowest torsion angles of the *dithione-M* and *dithiolate-M* coordination plane and to the π system extent of its dithiolate ligand, dmit, which confirms it to behave as an optimal candidate as donor in donor–acceptor mixed-ligand dithiolene complexes to achieve high second order NLO activity. It has been shown that the order of the above cited dithione torsion angle for this class of complexes correlates inversely with the oscillator strength and $\mu\beta_0$. The hyperpolarizability can be expressed as in eqn (2), in terms of the simple two-state model:[20]

$$\beta_{CT} = \frac{(\mu_e - \mu_g)\mu_{ge}^2}{\Delta E_{ge}^2} \quad (2)$$

where μ_e is the excited state dipole moment, μ_g is the ground state dipole moment, μ_{ge} is the transition state dipole moment and ΔE_{ge} is the transition energy between the two states. The favorable influence of the low torsion angle in Pr^i derivatives may balance the less favourable transition energy between the two states (see results from electrochemical experiments below) to achieve similar first molecular hyperpolarizabilities, as observed in corresponding metal complexes of the **1–3** and **4–6** triads.

In the solid state the bands relatable to the HOMO–LUMO transition are shifted to lower energy and a shoulder at lower energy accompanies this band, reflecting the influence of packing in electronic characteristics of these solids and enlarging their absorption range in the near infrared region, as shown for **6** in Fig. 8, and for **3**, **4** and **5** in Fig. S5 and S6.† The comparison of diffuse reflectance spectra of **3** and **6** is also reported in Fig. 9 and S7† for **2** and **5**. The shift to higher wavelengths of the shoulder in the NIR region (approximately 1280 nm for **3** and 1340 nm for **6**) is likely due to the additional π···π stacking interactions observed in the Bz derivative. Spectra of **1** and **4** are available in ref. 6, and show that no shoulder relatable to π stacking appears in **4**, in agreement with its solid state packing motifs. Recently the interesting spectroscopic properties of solids based on platinum diimine–dithiolato complexes alone or acting as donors towards nitrofluerenone acceptors have been investigated.[21] These solids, which exhibit continuous absorptions spanning from ultraviolet to near infrared, have been termed "black absorber" and are presented as materials of interest for molecule-based solar cells, given that red and NIR

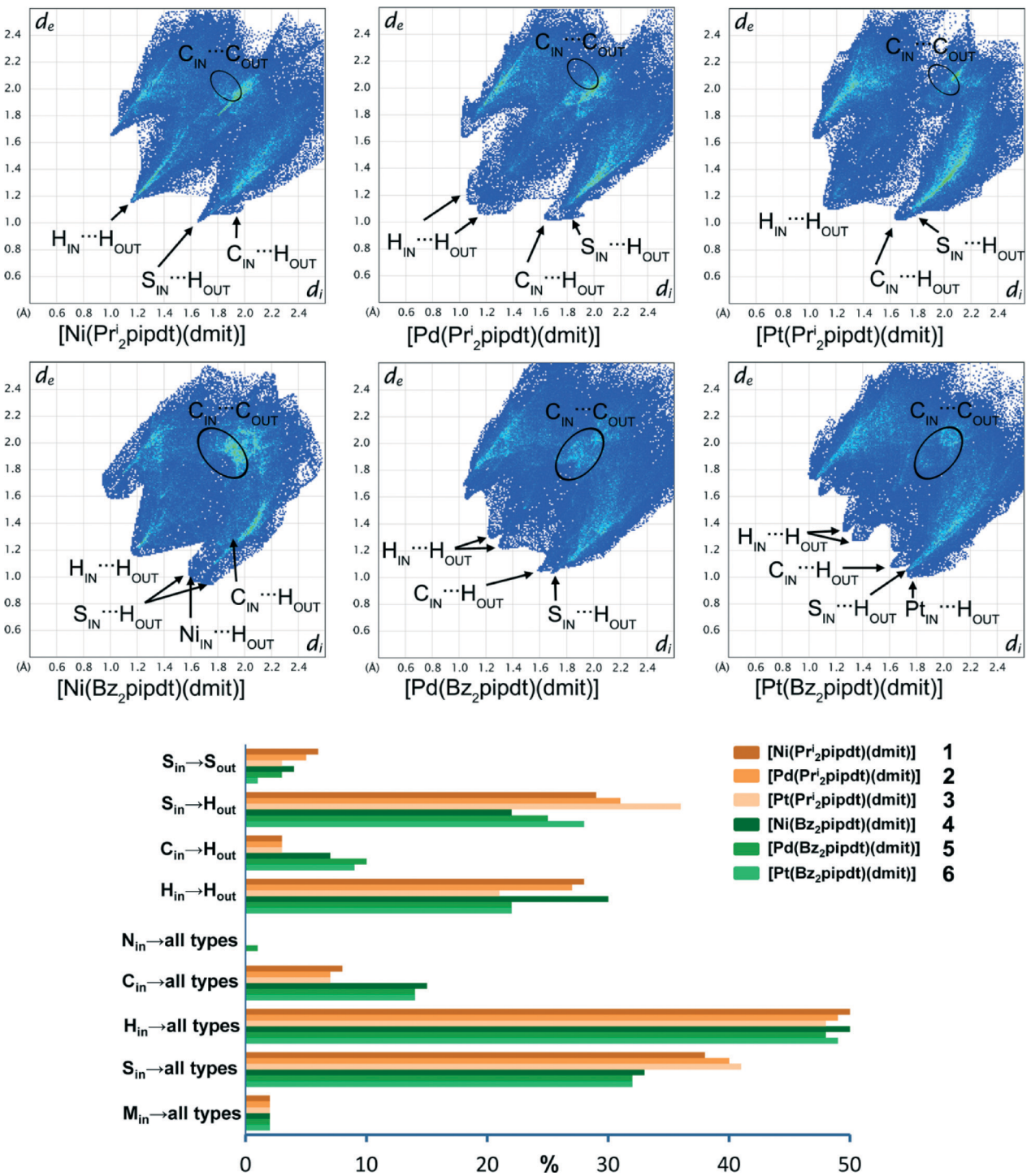

Fig. 7 Above, fingerprint plots of the complexes [M(Bz$_2$pipdt)(dmit)] and [M(Pr$^i_2$pipdt)(dmit)] (M = Ni, Pd, Pt); d_e and d_i represent the distance from the Hirshfeld surface to the nearest nucleus outside or inside, respectively, the surface. Color codes varying from blue to red highlight the frequency with which a (d_e, d_i) is observed. Below, percentage contribution of the various intermolecular contacts exchanged by [M(Bz$_2$pipdt)(dmit)] and [M(Pr$^i_2$pipdt)(dmit)] (M = Ni, Pd, Pt) with the surrounding environment reported as coloured bars as derived from the fingerprint plot analysis.

photons constitute more than 50% of the solar radiation.[21] The similarity of spectroscopic and of electrochemical and structural features of d^8 dithione–dithiolato complexes to those of diimine–dithiolato ones[1] makes these complexes promising candidates to be investigated for similar purposes.

Electrochemistry

Cyclic voltammetric experiments performed on DMF solutions of the complexes exhibit two reversible reduction waves and one irreversible oxidation wave as reported in Table 4.

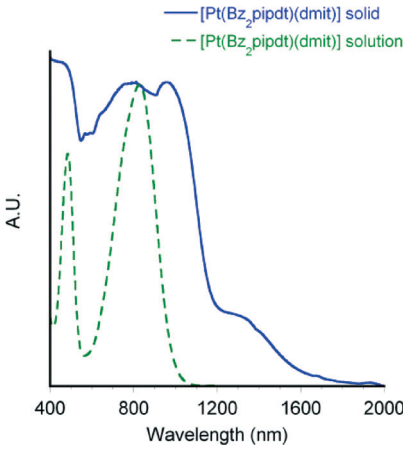

Fig. 8 Comparison of solid state diffuse reflectance (continuous line) and DFM solution spectra (dashed line) of **6** in arbitrary units.

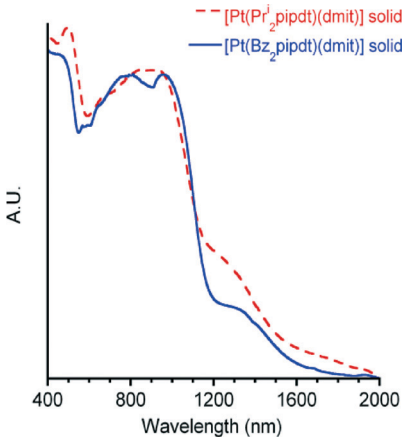

Fig. 9 Comparison of diffuse reflectance spectra of **3** (continuous line) and of **6** (dashed line).

The reduction processes occur at slightly more negative values with respect to those found for the corresponding Bz_2pipdt ligands (see CV scans in Fig. S8† as a representative example for **3**). The reduction processes are heavily influenced by the features of the LUMO. According to the prevalent contribution of the dithione ligand to this orbital, the less negative values for the reduction processes in Bz derivatives should be relatable to their higher capability to accommodate negative charges with respect to corresponding Pr^i ones.

The oxidation potential (E_a) is correlated to the ease of one electron of metal and dithiolate orbitals. Accordingly E_a should depend both on the metal and the dmit, and thus comparable E_a values are predictable for complexes having the same metal among the series. This happens for the Pd case only. However it must be the removal process from the HOMO, which is formed by a mixture, that remarked that the reason of the irreversibility of the oxidation process is not clear and may be related to the formation of insoluble or decomposition products. Thus the possible deposition of the oxidized species as a film on the electrode surface may alter the measured E_a values, hindering their reliability.

Table 4 Cyclic voltammetric data. Measured at the Pt electrode in DMF, 0.1 M Bu_4NBF_4 (reference electrode Ag/AgCl) for **1–3**. Corresponding data for **4–6** are reported for comparison (ref. 3*e*)

Complex	E_a[a] (V) 0 → +1	$E^1_{1/2}$ (V) 0 → −1	$E^2_{1/2}$ (V) −1 → −2
[Ni(Pr^i_2pipdt)(dmit)]	+1.01	−0.49	−1.04
[Pd(Pr^i_2pipdt)(dmit)]	+0.84	−0.38	−0.93
[Pt(Pr^i_2pipdt)(dmit)]	+0.71	−0.42	−0.96
[Ni(Bz_2pipdt)(dmit)]	+0.69	−0.41	−0.91
[Pd(Bz_2pipdt)(dmit)]	+0.84	−0.36	−0.81
[Pt(Bz_2pipdt)(dmit)]	+0.86	−0.39	−0.84

[a] Irreversible.

Conclusions

The [M(R_2pipdt)(dmit)] Ni–Pt triads based on donor/acceptor S,S′ ligands were investigated in order to assess the role of the functionalization of the pipdt ligand on the properties of the complexes. When substituting the isopropyl for the benzyl groups in the piperazine-2,3-dithione ligand, only minor changes are induced in their properties in solution, given their very similar molecular structures. Both **1–3** and **4–6** triads behave as redox active second-order NLO chromophores and exhibit comparably high negative molecular quadratic optical nonlinearity. Moreover studies on ultrafast excited-state dynamics of these complexes, investigated by transient absorption spectroscopy on the femtosecond–picosecond timescale, show a common photo-behavior for the two triads, although individual kinetic parameters and quantum yields can vary with the metal, the dithione ligand and the solvent.[22] On the other hand, different structural features are observed in their crystal packing upon changing R from Bz to Pr^i in the piperazine ring, and also, more surprisingly, inside the triads when changing the metal ion. In **1** and **2**, two complex molecules are stacked in a head-to-tail fashion forming a dimeric entity, whereas in **3** the complex molecules are

Table 3 Optical and EFISH results for **1–3**

Complex	λ_{max} (nm)	$\varepsilon \times 10^{-3}$ (M^{-1} cm^{-1})	$\mu\beta_\lambda$[a] (10^{-48} esu)
[Ni(Pr^i_2pipdt)(dmit)]	827 (707; 843)[b]	8.6	−6200
[Pd(Pr^i_2pipdt)(dmit)]	775 (700; 828)[b]	5.5	−4700
[Pt(Pr^i_2pipdt)(dmit)]	790 (731; 805)[b]	13.3	−7300

[a] In DMF, the uncertainty of the measure is between ±10%. [b] Determined by deconvolution of the above peak.

partially stacked above each other leading to the formation of supramolecular layers. The presence of the aromatic rings of Bz in **4–6** introduces the possibility of additional interactions in the solid state such as π···π stacking and CH···π interactions. Moreover, the conformational flexibility of the benzyl residue gives rise to different arrangements of the benzyl residues of pipdt with respect to the molecular plane. The benzyl groups may be oriented on the same side, as in **4**, or on opposite sides, as in **5**/**6**. These additional degrees of freedom are not present in **1–3**, where the i-propyl residues adopt a unique conformation that minimizes the steric hindrance between the methyl groups and the molecular plane. According to the Hirshfeld surface analysis a good portion of the interactions exchanged by the complexes are those occurring between the hydrogen atoms with the surrounding molecules, followed by the interactions exchanged by the sulphur atoms. The third main type of interaction is that involving the carbon atoms. There is however a distinctive pattern that differentiates **1–3** from **4–6**. In particular, the interactions involving the sulphur atoms are more important for **1–3** than for **4–6**, while a significant fraction of the interactions comprises the carbon atoms in **4–6**. This is in agreement with the presence of a significant number of π···π and CH···π interactions exchanged by the benzyl residues. Intermolecular interactions shift to higher wavelengths that are the absorbance range of these solids, which spans from the ultraviolet to the near infrared region, making these compounds of interest as redox active "black" absorbers.

Acknowledgements

Università degli Studi di Cagliari and Fondazione Banco di Sardegna are acknowledged for financial support to this research. Cooperation between Italian and French teams was developed inside COST-Action D35.

L. P. thanks the FP-7 PEOPLE-Marie Curie Intra European Programme and gratefully acknowledges Sardinia Regional Government for the financial support (P.O.R. Sardegna F.S.E. Operational Programme of the Autonomous Region of Sardinia, European Social Fund 2007–2013 - Axis IV Human Resources, Objective l.3, Line of Activity l.3.1 "Avviso di chiamata per il finanziamento di Assegni di Ricerca").

References

1 (*a*) *Dithiolene Chemistry: Synthesis, Properties, and Applications, in the Series Progress in Inorganic Chemistry*, ed. E. I. Steifel and K. D. Karlin, John Wiley & Sons, Hoboken, New Jersey, vol. 52, 2004; (*b*) P. Deplano, L. Pilia, D. Espa, M. L. Mercuri and A. Serpe, *Coord. Chem. Rev.*, 2010, **254**, 1434–1447; (*c*) P. Deplano, M. L. Mercuri, A. Serpe and L. Pilia, chapter 16 in the book *The Chemistry of Metal Enolates*, ed. J. Zabicky, John Wiley & Sons, Chichester, 2009; (*d*) F. Bigoli, C.-T. Chen, W.-C. Wu, P. Deplano, M. L. Mercuri, M. A. Pellinghelli, L. Pilia, G. Pintus, A. Serpe and E. F. Trogu, *Chem. Commun.*, 2001, 2246–2247.

2 (*a*) C.-T. Chen, S.-Y. Liao, K.-J. Lin and L.-L. Lai, *Adv. Mater.*, 1998, **3**, 334; (*b*) ed. S. D. Cummings, R. Eisenberg and E. I. Stiefel, Dithiolene Chemistry: Synthesis, Properties and Applications, *Progress in Inorganic Chemistry*, Wiley, Chichester, 2004, vol. 52, pp. 315–367; (*c*) C. A. Mitsopoulou, *Coord. Chem. Rev.*, 2010, **254**, 1448–1456; (*d*) C. Makedonas and C. A. Mitsopoulou, *Eur. J. Inorg. Chem.*, 2006, 590.

3 (*a*) S. Curreli, P. Deplano, C. Faulmann, A. Ienco, C. Mealli, M. L. Mercuri, L. Pilia, G. Pintus, A. Serpe and E. F. Trogu, *Inorg. Chem.*, 2004, **43**, 5069; (*b*) D. Espa, L. Pilia, L. Marchiò, M. Pizzotti, N. Robertson, F. Tessore, M. L. Mercuri, A. Serpe and P. Deplano, *Dalton Trans.*, 2012, **41**, 12106–12113; (*c*) D. Espa, L. Pilia, L. Marchiò, F. Artizzu, A. Serpe, M. L. Mercuri, D. Simão, M. Almeida, M. Pizzotti, F. Tessore and P. Deplano, *Dalton Trans.*, 2012, **41**, 3485–3493; (*d*) L. Pilia, D. Espa, A. Barsella, A. Fort, C. Makedonas, L. Marchiò, M. L. Mercuri, A. Serpe, C. A. Mitsopoulou and P. Deplano, *Inorg. Chem.*, 2011, **50**, 10015–10027; (*e*) D. Espa, L. Pilia, L. Marchiò, M. L. Mercuri, A. Serpe, A. Barsella, A. Fort, S. J. Dalgleish, N. Robertson and P. Deplano, *Inorg. Chem.*, 2011, **50**, 2058.

4 D. Espa, L. Pilia, C. Makedonas, L. Marchiò, M. L. Mercuri, A. Serpe, A. Barsella, A. Fort, C. Mitsopoulou and P. Deplano, *Inorg. Chem.*, 2014, **53**, 1170.

5 (*a*) C. Faulmann, A. Errami, B. Donnadieu, I. Malfant, J.-P. Legros, P. Cassoux, C. Rovira and E. Canadell, *Inorg. Chem.*, 1996, **35**, 3856; (*b*) R. Kato, *Chem. Rev.*, 2004, **104**, 5319–5346; (*c*) J. Lieffrig, O. Jeannin, P. Auban-Senzier and M. Fourmigué, *Inorg. Chem.*, 2012, **51**, 7144; (*d*) M. Nihei, H. Tahira, N. Takahashi, Y. Otake, Y. Yamamura, K. Saito and H. Oshio, *J. Am. Chem. Soc.*, 2010, **132**, 3553; (*e*) X.-R. Chen, W.-H. Ning, H. Yang, J.-L. Liu, F. Xuan and X.-M. Ren, *Dalton Trans.*, 2014, **43**, 6251.

6 E. A. M. Geary, L. J. Yellowlees, S. Parsons, L. Pilia, A. Serpe, M. L. Mercuri, P. Deplano, S. J. Clark and N. Robertson, *Dalton Trans.*, 2007, 5453–5459.

7 J. J. McKinnon, D. Jayatilaka and M. A. Spackman, *Chem. Commun.*, 2007, 3814–3816.

8 SMART (control) and SAINT (integration) software for CCD systems, Bruker AXS, Madison, WI, USA, 1994.

9 (*a*) N. Walker and D. Stuart, *Acta Crystallogr., Sect. A: Found. Crystallogr.*, 1983, **39**, 158; (*b*) F. Ugozzoli, *Comput. Chem.*, 1987, **11**, 109.

10 *Area-Detector Absorption Correction, SADABS*, Bruker AXS Inc., Madison, WI, USA, 2001.

11 A. Altomare, M. C. Burla, M. Camalli, G. L. Cascarano, C. Giacovazzo, A. Guagliardi, A. G. G. Moliterni, G. Polidori and R. Spagna, SIR97: a new tool for crystalstructure determination and refinement, *J. Appl. Crystallogr.*, 1999, **32**, 115–119.

12 G. M. Sheldrick, *SHELX97. Programs for Crystal Structure Analysis*, University of Göttingen, Germany, 1997, (Release 97-2).

13 L. J. Farrugia, WinGX and ORTEP for Windows: an update, *J. Appl. Crystallogr.*, 2012, **45**, 849–854.

14 C. F. Macrae, I. J. Bruno, J. A. Chisholm, P. R. Edgington, P. McCabe, E. Pidcock, L. Rodriguez-Monge, R. Taylor, J. van de Streek and P. A. Wood, Mercury CSD 2.0 - new features

for the visualization and investigation of crystal structures, *J. Appl. Crystallogr.*, 2008, **41**, 466–470.

15 M. A. Spackman and D. Jayatilaka, *CrystEngComm*, 2009, **11**, 19–32.

16 S. K. Wolff, D. J. Grimwood, J. J. McKinnon, M. J. Turner, D. Jayatilaka and M. A. Spackman, *CrystalExplorer*, University of Western Australia, 2012.

17 M. A. Spackman and J. J. McKinnon, *CrystEngComm*, 2002, **4**, 378–392.

18 L. Pilia, F. Artizzu, C. Faulmann, M. L. Mercuri, A. Serpe and P. Deplano, *Inorg. Chem. Commun.*, 2009, **12**, 490.

19 (*a*) E. Cariati, M. Pizzotti, D. Roberto, F. Tessore and R. Ugo, *Coord. Chem. Rev.*, 2006, **250**, 1210–1233; (*b*) K. D. Singer, E. Sohn, L. A. King, H. M. Gordon, H. E. Katz and P. W. Dirk, *J. Opt. Soc. Am. A*, 1989, **B6**, 1339.

20 (*a*) J. L. Oudar and D. S. Chemla, *J. Chem. Phys.*, 1977, **66**, 2664; (*b*) S. Bruni, E. Cariati, F. Cariati, F. A. Porta, S. Quici and D. Roberto, *Spectrochim. Acta, Part A*, 2001, **57**, 1417.

21 C. Browning, J. M. Hudson, E. W. Reinheimer, F.-L. Kuo, R. N. McDouglad Jr., H. Rabaâ, H. Pan, J. Bacsa, X. Wang, K. R. Dunbar, N. D. Sheperd and M. A. Omary, *J. Am. Chem. Soc.*, 2014, **136**, 16185.

22 F. Frei, A. Rondi, D. Espa, M. L. Mercuri, L. Pilia, A. Serpe, A. Odeh, F. Van Mourik, M. Chergui, T. Feurer, P. Deplano, A. Vlček Jr. and A. Cannizzo, *Dalton Trans.*, 2014, **43**, 17666–17676.